Title:

Exceptional preservation of three-dimensional dunes on an ancient deep-marine seafloor: implications for sedimentary processes and depositional environments

Authors: Euan L. Soutter[1], Ander Martínez-Doñate[1], Ian A. Kane[1], Miquel Poyatos-Moré[2], William Taylor[3], David Hodgson[3], Max J. Bouwmeester[1] and Stephen Flint[1]

Institutions: [1]Department of Earth and Environmental Science, University of Manchester, Manchester, M13 9PL, United Kingdom

[2]Departament de Geologia, Universitat Autònoma de Barcelona, 08193 Cerdanyola del Vallés. Spain

[3]School of Earth and Environment, University of Leeds, Leeds, LS2 9JT, United Kingdom

Correspondence: Euan L. Soutter (euan.soutter@manchester.ac.uk)

Abstract

Depositional and erosional bedforms can be used to reconstruct sedimentary processes and aid paleoenvironmental interpretations. Using exhumed deep-marine strata in the Eocene Aínsa Basin, Spain, we document a 3-dimensional package of dunes; a relatively rarely identified bedform in deep-marine environments. Our analysis shows that the dunes have curvilinear crests in planform, with smaller superimposed dunes and ripples deflected across the dune stoss sides. Beds containing these dunes have two main internal divisions: a lower inversely-graded (fine-to-coarse sandstone) and predominantly structureless division, and an upper coarse-grained sandstone division with well-developed cross-stratification, which is scoured and mantled with mudclasts and coarse-grains on the stoss-side. Following recently reported direct measurements of natural turbidity currents, we interpret the basal division as recording deposition from the dense basal head of a high-velocity turbidity current, followed by the development of dunes beneath the more sustained but still relatively high-velocity flow body that reworked the initial sandy deposit into downstream migrating dunes and scours. These dune-forming beds have been identified in different deep-water environments in the Aínsa Basin, including channel overbank and channel mouth settings and scour-fills. This indicates that the dunes are intimately tied to high-velocity flows that bypass through channel axes before becoming depositional during flow expansion across the channel overbank or at the channel mouth. Preservation of these dunes in the Aínsa Basin was likely enhanced by tectonically-forced lateral migration of channels, which prevented cannibalisation of bypass-zones, high aggradation rates dues to confinement, or by periodic sourcing of flows from a particularly clay-poor entry point. Where identified at outcrop or in the subsurface, these deposits are, therefore, diagnostic of substantial and contemporaneous sediment bypass downslope and are important for predicting the timing of sediment delivery to deep-water basins.

Keywords

Dunes, deep-marine, Pyrenees, Ainsa, turbidite

1. Introduction

Fluidal flows can deposit and entrain sediment as they flow over a moveable bed, forming a suite of erosional and depositional bedforms related to the properties of both the fluid and the bed. Since different sedimentary environments are associated with different prevailing flow conditions, assemblages of bedforms can be used to reconstruct paleoenvironments from the sedimentary record (e.g. Allen, 1982; Southard and Boguchwal, 1990; Reading, 2009; Collinson and Mountney, 2019). Placing greater constraints on the distribution of bedforms in sedimentary systems and the conditions under which various bedforms develop is therefore critical for accurate paleohydraulic and paleoenvironmental reconstructions (e.g. Leeder, 1983; Dumas et al. 2005). In deep-water settings, bedforms are typically formed by turbidity currents, which are turbulent mixtures of sediment and water that flow downslope due to their excess density (e.g. Kuenen and Miglorini, 1950; Sequeiros et al. 2010; Meiburg and Kneller, 2010), or by more dilute density currents, such as contour currents, where excess density is a consequence of temperature or salinity gradients in the ocean (e.g. Rodrigues et al. 2022). A wide variety of bedforms can form beneath these currents (e.g. Fedele et al. 2016; Cartigny and Postma, 2017), and they are commonly used to aid reconstructions of deep-water processes and environments in modern (e.g. Hage et al. 2018; Normandeau et al. 2020) and ancient (e.g. Komar, 1985; Baker and Baas, 2020) sedimentary systems.

Dunes, which migrate downstream by erosion of an upstream-facing stoss-side and deposition on a downstream-facing lee-side, should precede ripples in the stratigraphic record of an 'ideal' decelerating sandy turbidity current (Bouma, 1962; Tilston et al. 2015), and therefore be relatively common in turbidity current deposits, known as 'turbidites'. Deep-water dunes, however, are rarely identified, which has attracted interest for decades (e.g. Walton, 1967; Arnott, 2012). The relative paucity of dunes compared to other bedforms in turbidites has been attributed to; 1) turbulent flows having deposited their coarse grains prior to entering the dune-forming velocity and grain size phase (Walton, 1967), 2) high flow densities and sedimentation rates in the dune-forming velocity phase suppressing dune formation (Lowe, 1988; Arnott, 2012), 3) a lack of time spent in the dune-forming phase (Walker, 1965; Pickering and Hiscott, 1995), 4) high clay contents altering the flow and/or bed rheology (Simons et al. 1963; Baas and Best, 2002; Schindler et al. 2015), and 5) the narrow grain size range capable of generating steep enough density gradients to create the angular bed defects required for dune development (Tilston et al. 2015). Preservation potential may also be an issue, with the high-velocity flows necessary for dune formation likely associated with net-erosional environments, such as channels (e.g. Conway et al. 2012), which may result in dunes being frequently formed but eroded. Dunes are therefore only sporadically identified in exhumed deep-water sedimentary basins when compared with other bedforms and other sedimentary environments (e.g. Bouma, 1962; Ricci Lucchi & Valmori, 1980, Pickering and Hiscott, 1995; Amy et al. 2000; Kneller and McCaffrey, 2003; Sumner et al. 2012; Stevenson et al. 2015). Consequently, the conditions required for dune formation and preservation, their internal structure, and their paleogeographic significance in deep-water environments remain relatively poorly constrained.

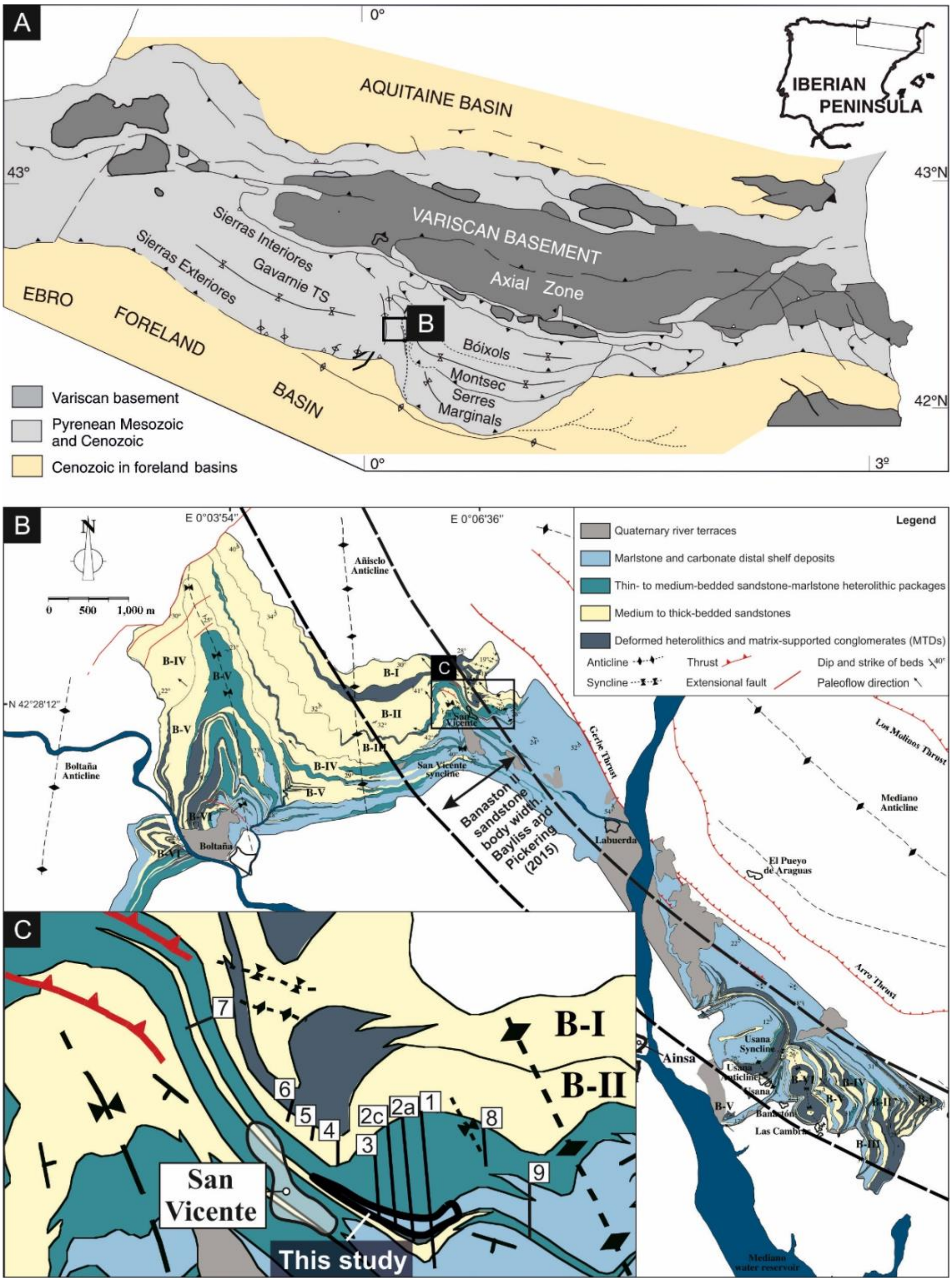

Figure 1. A) Geological map of the Pyrenees. This study focussed on the Cenozoic part of the foreland basin fill. **B)** Geological map of the deep-marine Banastón system within the Cenozoic Aínsa depocentre (modified from Bayliss and Pickering 2015). This study focuses on an interval within Banastón II (modified from Martínez-Doñate et al. 2023). **C)** Geological map of the study area (modified from Pickering and Bayliss, 2009; Bayliss and Pickering, 2015; Martínez-Doñate et al. 2023).

82

Here, we document an example of sandstone dunes within the deep-marine Eocene Aínsa depocentre, south Pyrenean foreland basin (Fig. 1), in which excellent exposure allows for detailed descriptions and quantification of dune-field morphology and internal characteristics. We aim to collate previous studies that have documented and discussed dunes of this style elsewhere in the Aínsa depocentre (Mutti et al. 1977; Mutti and Normark, 1987; Bakke et al. 2008; Cornard and Pickering, 2019; Tek et al. 2020), by discussing the origin, processes and paleogeographic significance of these packages explicitly, and in light of direct measurements of modern turbidity currents.

2. The Aínsa Depocentre and the Banastón System

The Aínsa depocentre is interpreted to represent the submarine slope segment (during the lower to middle Eocene) of the SE-NW trending south Pyrenean foreland basin and has been the subject of decades of research (Fig. 1A) (e.g. van Lunsen, 1970; Mutti, 1977; Puigdefàbregas and Souquet, 1986; Pickering and Bayliss, 2009; Fernández et al. 2012; Mochales et al. 2012; Castelltort et al. 2017; Cantalejo et al. 2021ab). Seven different sandstone-rich turbidite systems have been mapped within the basin-fill, each related to either tectonic uplift in the hinterland and subsidence in the depocentres or climatic and glacio-eustatic fluctuations (e.g. Pickering and Bayliss, 2009; Castelltort et al. 2017; Cantalejo et al. 2021a; Läuchli et al. 2021).

This study focuses on the Banastón system, which was deposited over ~2 Myr during the Lutetian (Cantalejo et al. 2021b) and is interpreted as a series of channel-levée-overbank complexes that reach a thickness of 700 m on the lower slope (Bayliss and Pickering, 2015). In particular, we focus on Banastón II, a sand-rich unit within the larger Banastón system that was topographically steered through the NW-trending basin by syn-depositional deformation of NE and SW laterally confining basin margins and mass-transport deposits (Fig. 1B)

(Pickering and Bayliss, 2015; Martínez-Doñate et al, 2023). The package of interest is interpreted to represent the overbank of a channel confined by an actively-deforming basin margin (Martínez-Doñate et al, 2023).

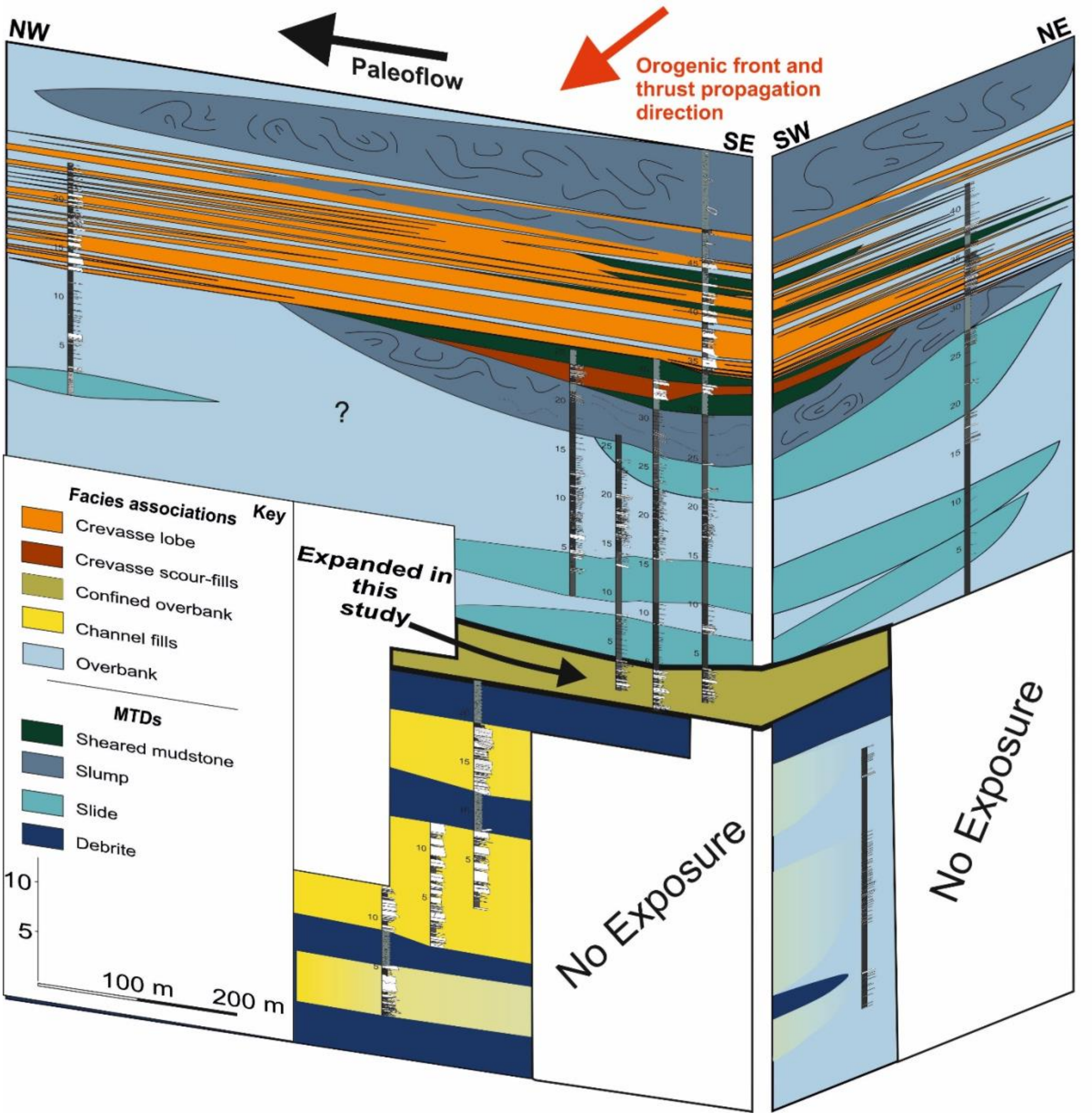

Figure 2. Correlation panel showing the depositional elements and stratigraphic evolution of the Banastón II system (modified from Martínez-Doñate et al. 2023). The interval of interest is highlighted in black and is interpreted as the confined overbank of an adjacent channel to the ~SW.

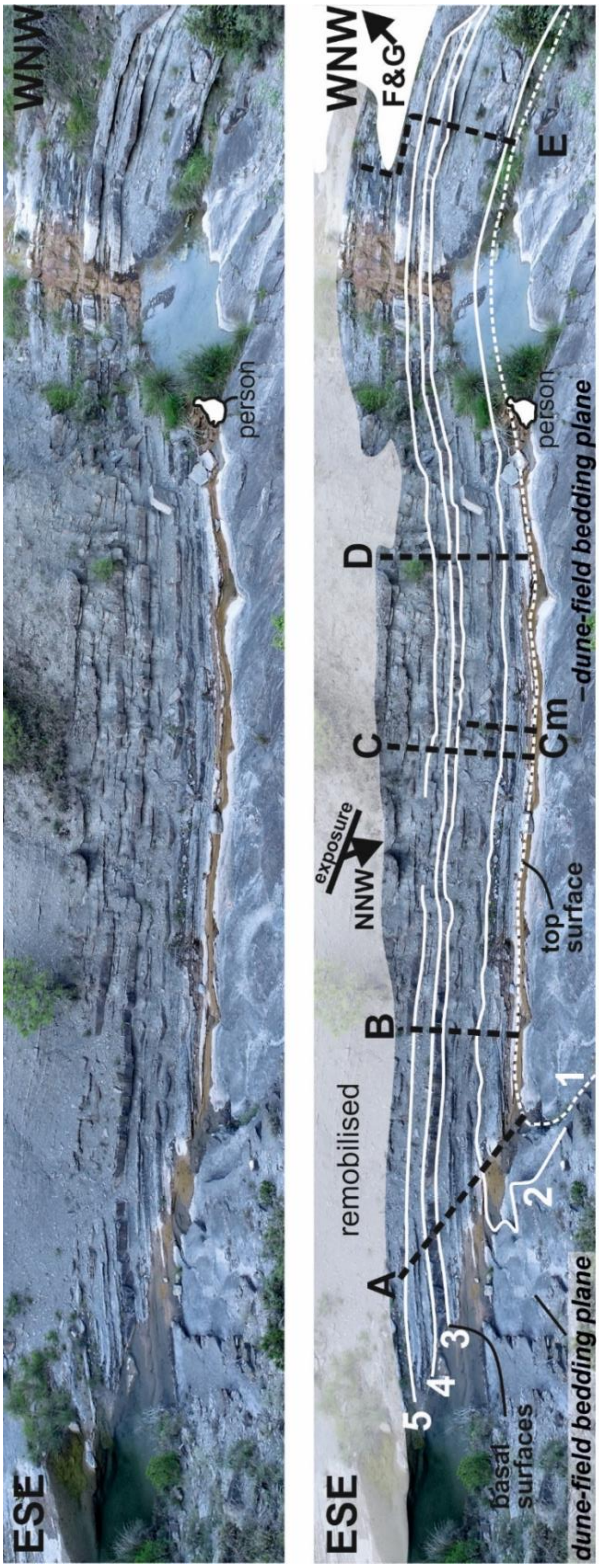

Figure 3. The interval of interest studied in-depth here, and the measured sections used to describe the sedimentology of the interval. A person is sitting on a well-exposed dune-field, which has the same facies as the cross-stratified beds within the measured sections.

3. Methods

The locality lies ~270 m east of San Vicente (42.4675°, 0.111944°) and forms part of the study by Martínez-Doñate et al (2023), who investigated the larger-scale evolution of the Banastón II system in this region (Fig. 1C; 2). This study focuses on the detailed characterisation of a specific part of this succession using additional data.

Eight sections (26 m cumulative) from the deposits of interest within the succession were measured at a 1:5 scale to capture centimetre-scale sedimentary features and were correlated by walking individual beds and Uncrewed Aerial Vehicle (UAV) photogrammetry to capture thickness and sedimentary facies variations (Fig. 3; 4; 5). The morphology of part of the dune-field was also measured using LiDAR (laser imaging, detection, and ranging) (Fig. 7).

Bedform orientation measurements (n = 244) were collected through the downstream axes of seven dunes exposed on a bedding plane (Fig. 6). Measurements at 5 cm intervals along these bedding planes allowed seven dune axis profiles to be calculated via trigonometry. Axial planes through each dune were used to reconstruct the dominant migration direction. Paleocurrents were collected from sole marks (flutes and grooves) and ripple and dune foresets throughout the interval of interest (n = 47). Five samples were collected at regular intervals through a representative bed with coarse-grained dunes. Petrographic analysis (point-counting of 200 points per sample) allowed vertical grain size and sorting trends to be assessed (Fig. 9).

135

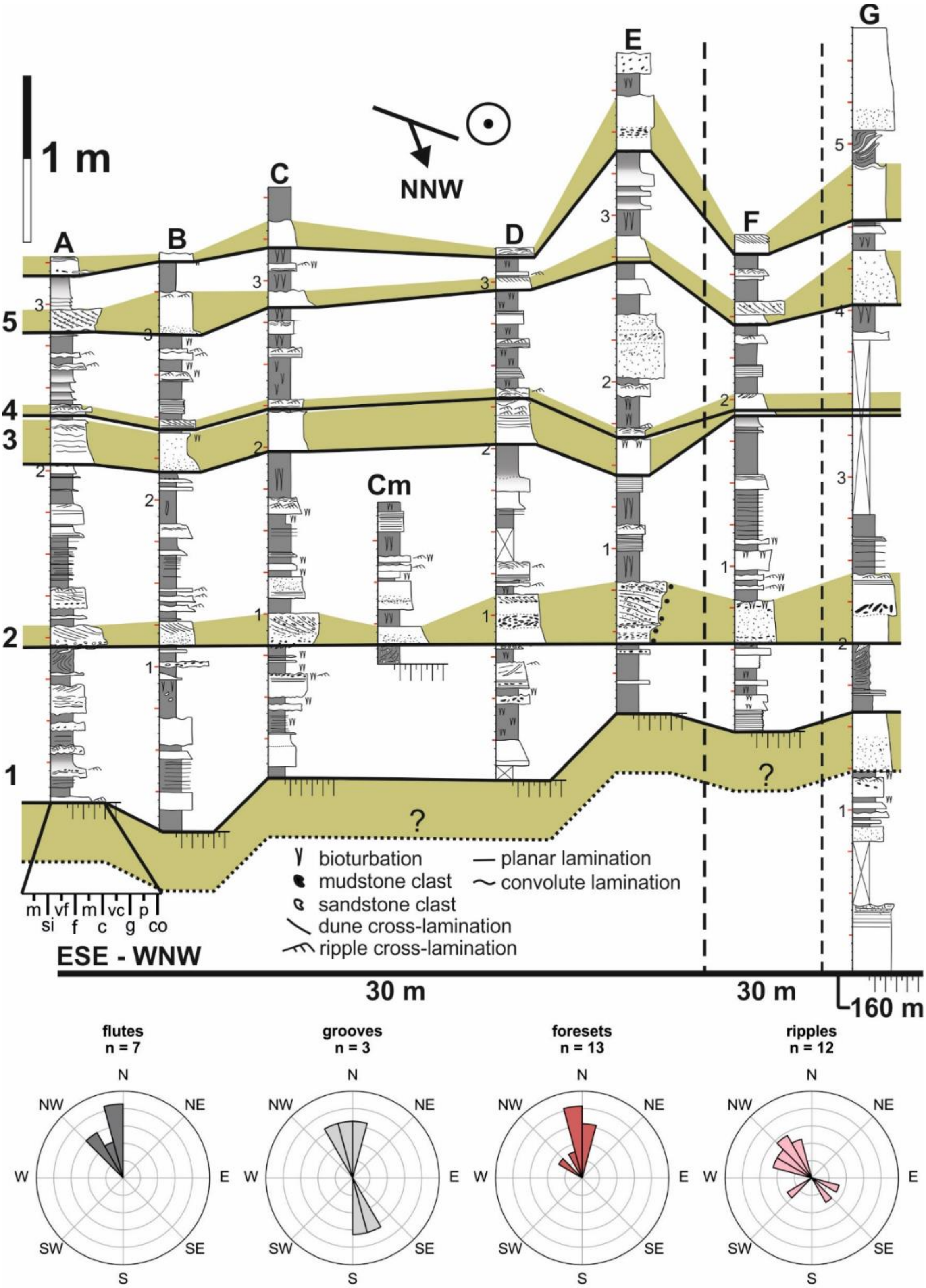

Figure 4. Measured sections from Figure 3 and paleocurrent rose diagrams. Coarse-grained, cross-stratified marker beds are highlighted in green. Foreset measurements from dunes and superimposed dunes preserved on the key bedding plane are analysed separately (Fig. 6).

4. Results

4.1. Paleocurrents

Sole-mark and foreset orientations are dominantly oriented toward the NW and NNW, consistent with paleoflow measured throughout the Banastón system (Bayliss and Pickering, 2009) and the deep-marine Aínsa Basin more broadly (e.g. Pickering and Bayliss, 2009) (Fig. 4; 6). Dunes superimposed on larger dunes show divergence from this pattern, with foresets tr?ending toward the NE and SW (Fig. 6). Ripples also show some divergence from the sole marks, being dominantly oriented to the NW and sometimes showing complete reversal toward the SE (Fig. 4). No upslope-accreting bedforms were observed.

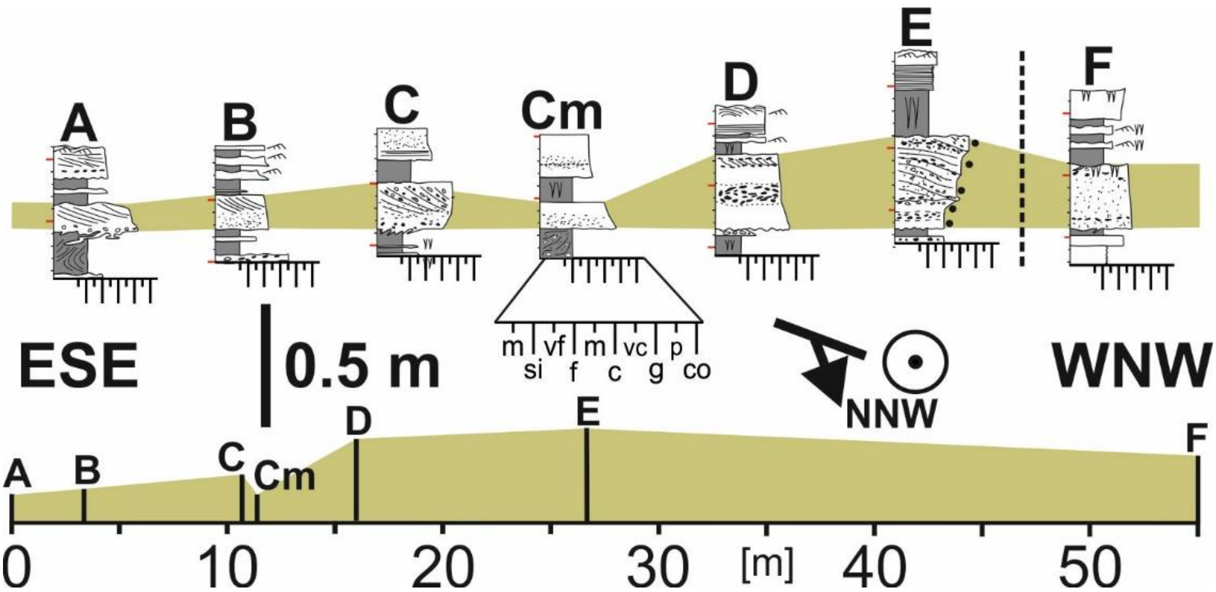

Figure 5. Sedimentology of a key marker bed with well-developed dunes (upper) and its true horizontal thickness variation (lower). Same as Fig. 4.

4.2. Sedimentary facies

The typical vertical sequence of the dune-forming beds begins with an erosion surface that cuts into the underlying fine-grained substrate, overlain by a structureless or faintly planar-laminated basal division (Fig. 4; 5; 8). This division may pass vertically into a mud- and lithoclast-rich division across an amalgamation surface that is more heavily weathered when dominated by mud-clasts and better preserved when dominated by lithoclasts or may be immediately overlain by coarse-grained foresets (Fig. 8), often with abundant *Nummulites*. The lithoclasts are extra-basinal and derived from the hinterland. Where the clast-rich division is present, the overlying foresets download and taper out within it. These foresets are commonly overlain by a fine-grained, ripple-laminated division, which infills depositional relief present on the foreset bedform and forms a grain-size break with the underlying coarse-grained foresets. Fine-grained intervals and other abrupt grain-size breaks are not observed in the foresets, supporting deposition under a single event. The bed tops are heavily bioturbated by horizontal, tube-like burrows, identified as *Thalassinoides*, that branch at approximately 90° (Fig. 8). Bed tops are commonly also mantled by patches of coarse grains and small mud clasts (< 2 cm), which occur in spoon-shaped scours. These beds also have a distinct reddish colour compared to beds within the underlying and overlying packages (Martínez-Doñate et al, 2023).

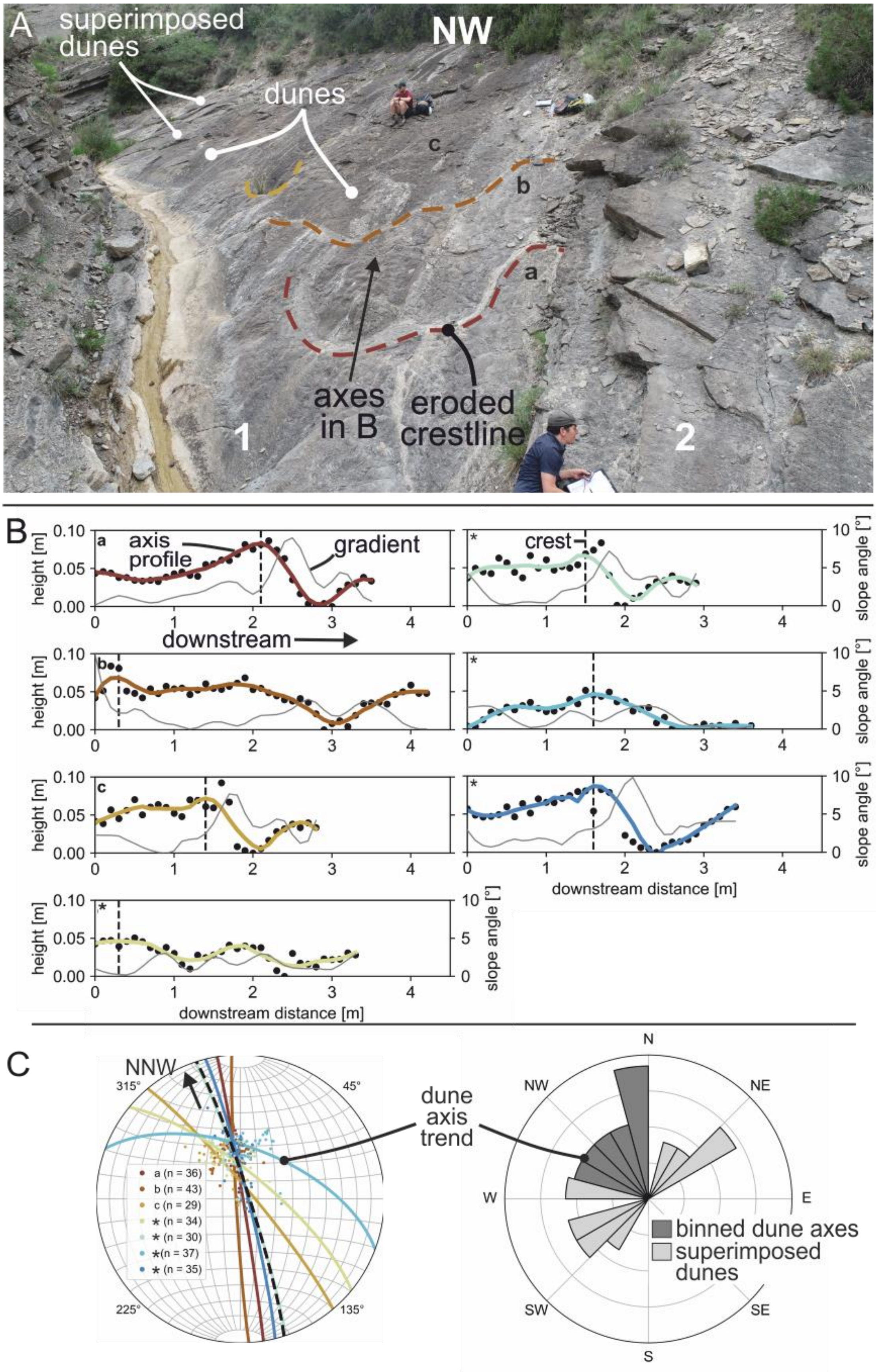

Figure 6. A) Bedding plane with curvilinear dunes and spoon-shaped scours. Exposure in Fig. 3 to the left. **B)** Downstream dune morphologies and gradients. Location of dune crestlines a, b and c in A. Asterisk (*) indicates dune profile unclear in A due to perspective. C. Dune axis trends and associated rose diagram. Dunes predominantly migrate to the NNW, while superimposed dunes migrate toward the SW and NE.

Laterally, these beds show substantial textural and thickness variation over tens of centimetres, with divisions composed of prominent foresets passing into faintly cross-bedded or structureless divisions (Fig. 4). Shorter-wavelength thickness variation is also accommodated by relief present on the foresets (Fig. 8), with overlying beds thickening where foresets in the underlying bed taper out. On a more regional scale, these packages appear to show an overall thinning trend toward the NE, consistent with thinning of the Banastón II as a whole toward a NE-confining intrabasinal slope (Fig. 2) (Bayliss and Pickering, 2015; Martínez-Doñate et al. 2023).

Thin-bedded (< 0.1 m) and normally-graded (silt-to-fine-grained) beds occur between these coarse-grained beds, along with fine-grained mass-transport deposits that contain deformed thin-beds (see Martínez-Doñate et al. 2023 for full description).

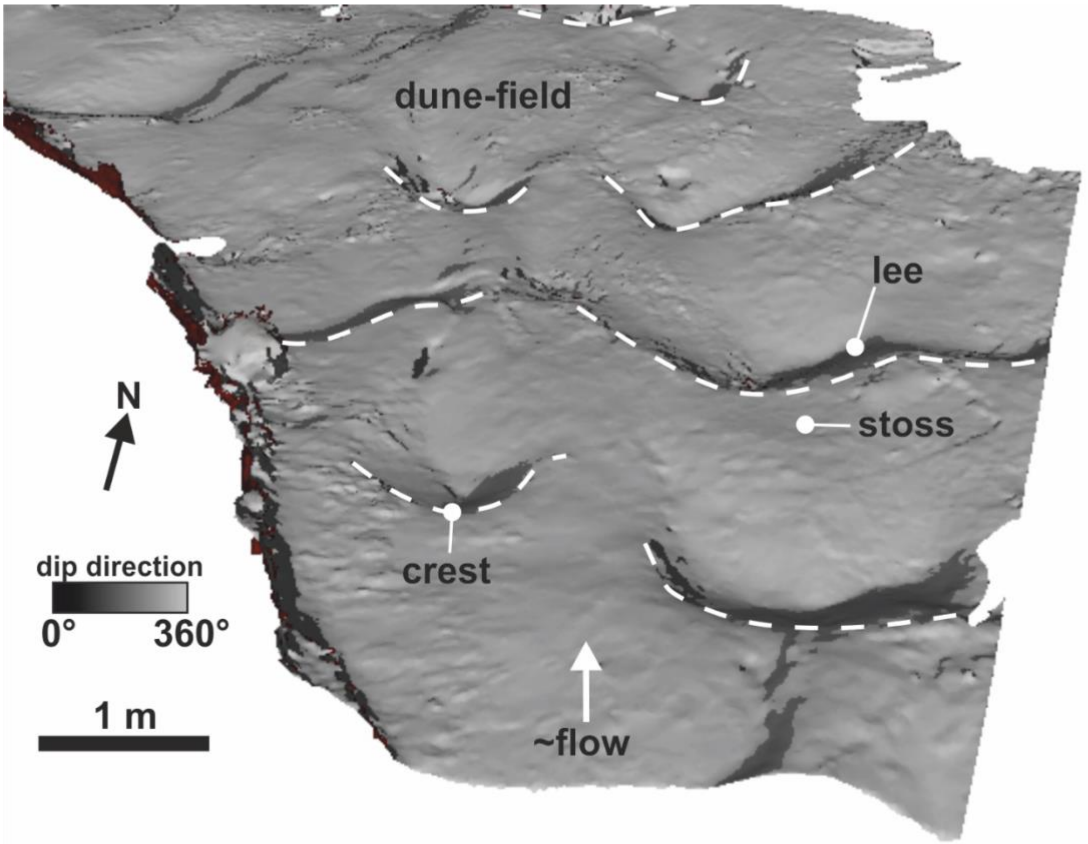

Figure 7. Lidar scan of part of the dune-field (Fig. 6A) coloured by dip-direction. Note steep downstream dipping lee-sides and shallow upstream-dipping stoss-sides. The sinuous shape of the dune crests and their tendency to merge along strike is also apparent.

4.3. Petrography

Point-counting indicates that the basal divisions of these beds are strongly inversely-graded, with median grain sizes passing from fine to coarse sand through the basal 5 cm (Fig. 9). The fine-grained sandstone base of this division also spans a much narrower grain size range than the coarse-grained top, which contains grain sizes from silt- to granule (Fig. 9). Samples from the foresets overlying this division are similarly coarse-grained with a wide grain size range (Fig. 9). Point-counting indicates little vertical variation in median grain size within the foresets when compared to the base of the bed, with visual measurements showing a weak inverse-grading from coarse to very coarse sand. Across the samples, sorting values fall between 0.8 and 1 Φ, indicating moderate sorting throughout the bed (Blair and McPherson, 1999). No obvious trends in sorting are observed from base to top; however, there is a negative correlation between sorting and grain size (Spearman rank correlation = -0.89, p-value = 0.04), indicating that sorting increases with increasing grain size (although with a very small sample size).

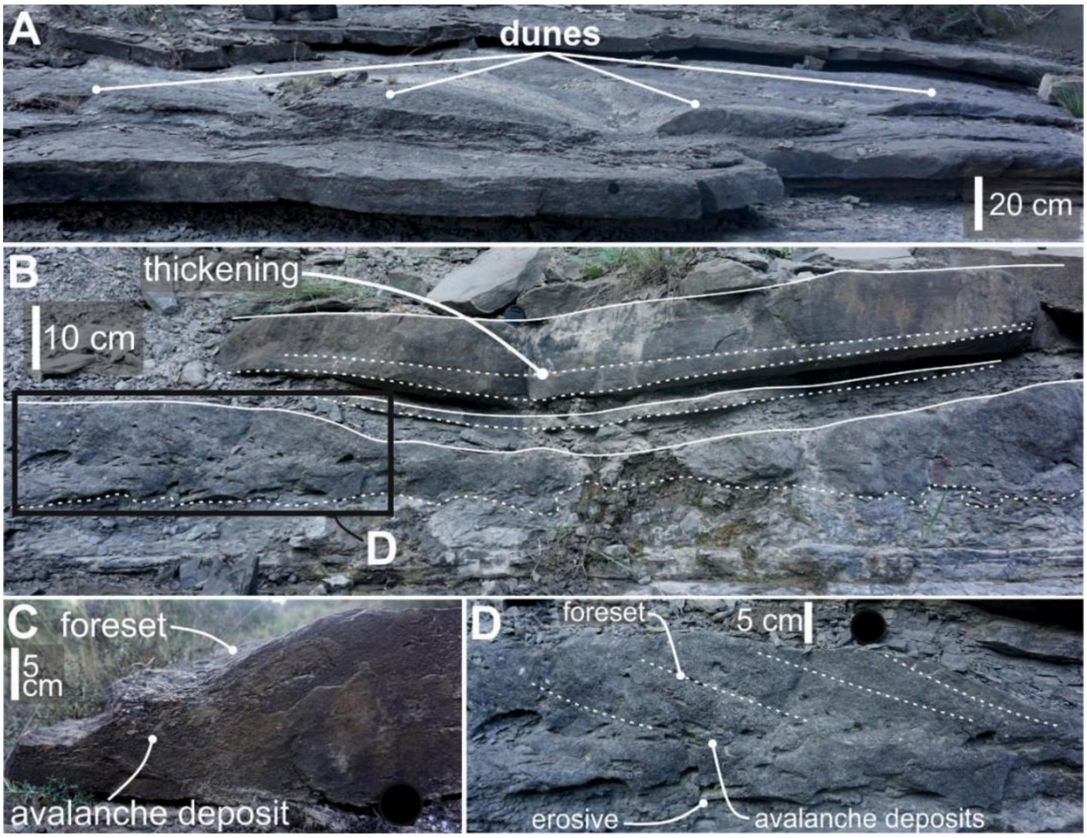

Figure 8. A) Dunes (label 2 on Fig. 6A) developed above more structureless division. B) Thickening of overlying beds into relief developed between dunes. C) Dune foreset and grain flow deposit formed via 'avalanching' down lee-slope. Grain flow deposits are composed of lithic and mudclasts. D) Zoomed view of B showing cross-stratification and grain flow deposits above more structureless and erosive division with mudclasts.

4.4. Dune morphology

Each measured dune has a wavelength (crest to next downstream crest along the axis of migration) of 1.5 to 2 m, with the distance between the crest and the trough varying between 0.5 m to 1 m (Fig. 6). Crest heights (relative to the trough) range between 0.05 - 0.1 m. Restored dune gradients are horizontal to 5° on stoss-slopes and up to 10° on lee-slopes. These (compacted) lee gradients are consistent with dunes formed by major rivers in the present, with 75% of fluvial dunes having lee-slopes of < 14.9° (Cisneros et al. 2020); however, migration of superimposed dunes, scouring and compaction will have modified the lee-slope (Fig. 8A). Spoon-shaped metre-wide scour surfaces are cut into the lee slope, and are mantled by mud clasts and coarse-grained sand lags. These surfaces shallow and widen downdip, with dunes inset to these erosion surfaces, with stoss-sides tending to have a lower elevation than stoss-sides immediately upslope, indicating coupled erosion and deposition during dune migration.

In planform view, the dunes have arcuate shapes and resemble barchan or lunate dunes commonly described in aeolian (e.g. Tsoar, 2001), shelfal (e.g. Todd, 2005), and, more rarely, in deep-marine settings, where they tend to be larger (10s to 100s of metres), finer-grained and formed by contour currents (e.g. Kenyon et al. 2002; Wynn et al. 2002; Miramontes et al. 2018) (Fig. 6). This shape appears to have been at least partially the result of scouring. Dune widths (from downstream crest tip to downstream crest tip across depositional-strike) range from 2 - 0.5 m. Superimposed dunes on the stoss-side are finer-grained and straight-crested (crest perpendicular to flow direction) (Fig. 6A). Ripples on the dune surface tend to be lunate in planform, as imaged on the stoss-side of barchan dunes on the present-day seafloor (Wynn et al. 2002).

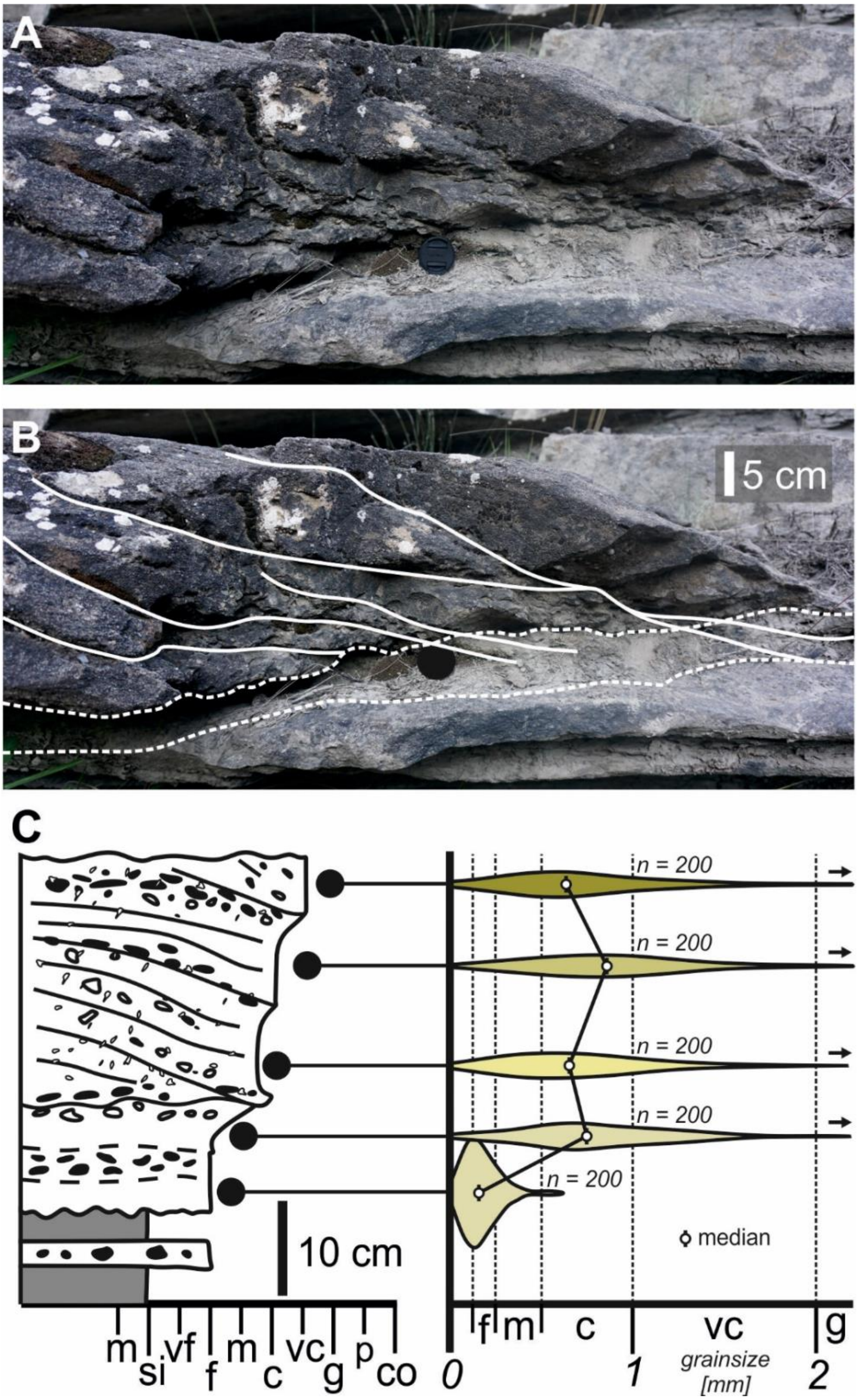

Figure. 9. A) Sampled bed (Fig. 5) and B) detailed measured section. Violin plots show grain sizes measured via point-counting. The inversely-graded basal division passes into a cross-stratified coarse-grained division.

216

5. Discussion

5.1. Flow processes

The deposition of a structureless, inversely-graded, and poorly-sorted division supports the initial passage of a high concentration flow (e.g. Lowe, 1982), which may have been deposited on a bedform larger than can be constrained at the outcrop. Inverse-grading likely reflects kinematic sieving and squeezing within the highly-concentrated basal layer, with fine grains ‘sieved’ downwards between coarse grains, and coarse grains ‘squeezed’ upwards by friction during transport (Le Roux, 2002). Inverse-grading can also be caused by coarse grains being transported more slowly than fine grains (e.g. Hand, 1997), or flow waxing, such as when turbidity currents are sourced directly by rivers (e.g. Mulder et al., 2021). Contemporaneous deposition of both low-density mudclasts and higher-density lithoclasts, along with a predominantly structureless sandy layer, indicates high rates of deposition and inhibited sorting, possibly due to flow capacity loss.

Reworking of this sandy layer into down-stream migrating dunes indicates that the flow evolved towards lower concentrations and reduced rates of deposition but still maintained high enough velocities and shear stresses to form dunes, possibly over a relatively long time period (Fig. 11). An alternative explanation may be that the flow was pulsed, or a separate and subsequent lower-concentration flow reworked the initial deposit; however the lack of a break between the basal division and the dune-prone division supports the passage of one flow.

Dune formation will have been promoted by the initial deposition of the sandy layer, as dune formation requires a substrate with a low clay content (Schindler et al. 2015). The presence of grain flow deposits and scouring at the foot of the lee-slope indicates flow separation at the bedform crest, supporting the interpretation of downstream migration (e.g. Sequeiros et al.

2010). Supercritical bedforms, such as antidunes, may have preceded the dunes; however, they will have been reworked into dunes and are, therefore, not preserved (de Cala et al. 2020). It should be noted that downstream-migrating dunes may form beneath supercritical flows (Fedele et al. 2016), precluding any estimates of flow criticality based on the presence of down-stream migrating dunes alone.

The presence of finer-grained dunes and ripples superimposed on the larger, primary dunes indicates further waning of the flow, resulting in the deposition of smaller, finer-grained bedforms. Divergence of the superimposed dune migration directions from the primary dune migration direction suggests that the waning flow was increasingly deflected across the stoss side of the primary dunes or deflected by mass-transport deposits or tectonic topography (Fig. 11). The superimposed dunes also have more linear crestlines than the underlying larger dunes, which is likely a consequence of reduced scouring and reworking on the stoss-sides of the smaller dunes. The final stage of flow evolution is represented by the upper fine-grained/silt division, which we interpret as deposited by the low-velocity tail of the flow, with shear stresses such that silt can settle, followed by ambient seawater conditions (Fig. 11). Differentiating the transition from turbiditic to hemipelagic deposition is difficult at the outcrop however, with apparently hemiplegic deposits observed to be composed almost entirely of microscopic turbidites in other deep-marine sediments (Boulesteix et al. 2019).

Spatially, these beds show tens of centimetres of thickness variation over tens of centimetres. Internal structures also vary spatially, transitioning from structureless to convolute laminated beds with multiple amalgamation surfaces and grain-size breaks (Fig. 4; 5). This abrupt variation in thickness and facies is likely a consequence of autogenic velocity fluctuations of the highly-energetic flows that deposited them, causing frequent transitions through the depositional and erosional boundary, both spatially and temporally (e.g. Ge et al. 2022).

Dune preservation is therefore limited to: 1) high-magnitude flows that are capable of sustaining high enough velocities to build dunes following deposition of their coarse load (e.g. Sylvester and Lowe, 2004), 2) flows with a coarse enough load to occupy the dune-building phase (e.g. Fedele et al. 2016), and 3) flows traversing a sandy substrate with little cohesive clay (Schindler et al. 2015). A lack of clay or fine silt could also result from periodic sourcing of the flows that produced these beds from a clay-poor environment; however, this is difficult to test without a detailed study linking facies with provenance across the basin. Assuming an approximately normal grain size distribution, these beds indicate major sediment bypass downslope, as finer-grained suspended sediment was continuously bypassed downstream during dune migration. The grain-size break between the coarse-grained dunes below and fine-grained ripples above supports this, with the missing grain-size fraction likely bypassed downslope (e.g. Stevenson et al. 2015), where thick mud caps are observed (Remacha and Fernández, 2003; Bell et al., 2018).

These observations and interpretations are consistent with direct measurements of present-day turbidity currents, which indicate that they are driven by a high-velocity thin and dense basal head that drives the migration of crescentic bedforms and knickpoints (Fig. 11) (Aspiroz-Zabala et al., 2017; Paull et al. 2018; Normadeau et al. 2020; Heijnen et al. 2020; Chen et al. 2021; Pope et al. 2022; Talling et al. 2022). The dense basal layer is followed by a more dilute body that slows as it thickens over hours to days (Aspiroz-Zabala et al., 2017; Pope et al. 2022). A similar flow structure is suggested to explain the dune-prone sandstone beds here, with the deposit of the dense basal layer reworked into dunes by the trailing body. Grain size and sorting variability within these dunes may reflect velocity fluctuations measured during the sustained passage of trailing flow bodies, as observed in turbidity currents of the Congo Canyon (Fig. 11) (Aspiroz-Zabala et al., 2017; Talling et al. 2022).

294

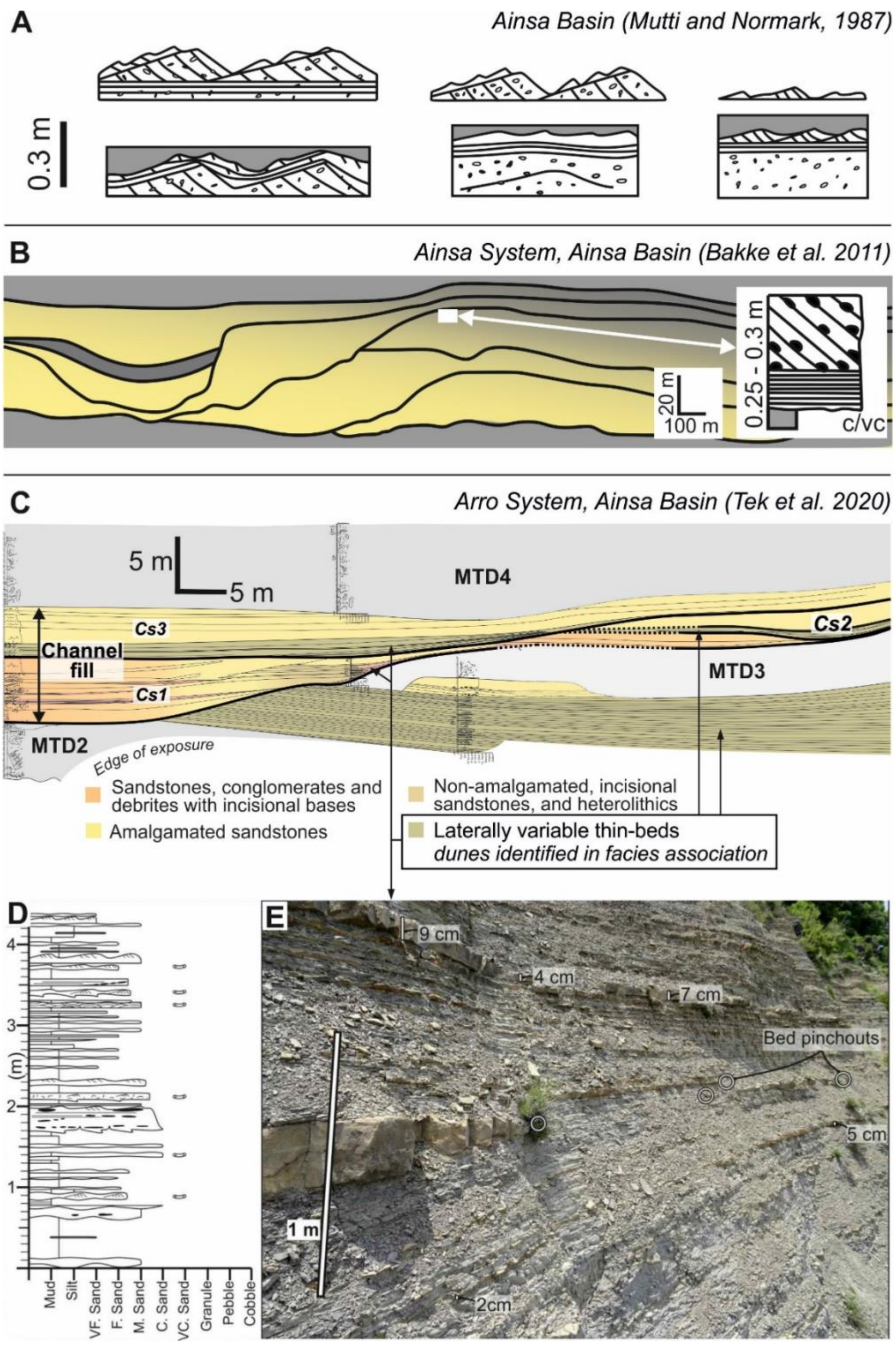

Figure 10. Examples of similar facies observed in other studies in the Aínsa Basin. **A)** Sketches of these facies across the Aínsa Basin (Mutti and Normark, 1987). **B)** Modified outcrop sketch of the Aínsa system used as a basis for a seismic model by Bakke et al. (2011) and the location of dune-like facies reported from their facies table. **C)** Correlation panel of an Arro system channel complex in the Aínsa Basin (modified from Tek et al. (2020). Dunes reported from the 'laterally variable thin beds' facies association by Tek et al. (2020). Cs; channel system, MTD; mass-transport deposit.

5.2. Dunes or pseudo-dunes

As Arnott et al. (2017) noted, cross-stratification may form through turbidity current deposition within seabed scours (‘pseudo-dunes’), with the resulting deposit resembling dunes constructed above the seabed. Some of the cross-stratified beds discussed here display features similar to those observed in pseudo-dunes where they transition laterally to structureless sandstones, overlie structureless sandstones and have erosive bases. The reddish colour of the pseudo-dune beds of Arnott et al. (2017) and some of the beds described here are also comparable. Arnott et al. (2017) ascribed the colouration to early diagenesis and ferric-cementation due to relatively high depositional porosity and permeability. These beds have also been observed to be associated with scours elsewhere in the basin (Bakke et al. 2008). However, some of the sandstones in the studied package have positive seabed relief (Fig. 6; 7), indicating they were constructed above the seabed and are, therefore, depositional bedforms.

It is possible that both pseudo-dune and dune formation occurred contemporaneously, as the high-magnitude flows responsible for the deposition of these coarse-grained beds would have been capable of contemporaneous scouring and forming dunes. The cross-stratification observed in some beds may therefore have been formed via scour-fill processes, while others are the product of dune-building. It is often difficult to differentiate between these owing to the scale of the outcrop compared to the potential scale of seabed scours (tens of metres to kilometres, see Hofstra et al., 2015, for compilation of scour dimensions) and the impacts of compaction on deposits of varying grain size distorting primary depositional architectures.

On a lower resolution dataset, such as bathymetric data, these dune fields may be entirely unresolved within such large scours, or perhaps resemble upstream-migrating crescentic bedforms formed by transcritical (alternating between supercritical and subcritical) turbidity currents (e.g. Hage et al, 2018; Normandeau et al, 2020). In such cases the lee-slopes of the crescentic bedforms may be in fact aggrading and migrating downslope, and not being eroded and migrating upslope, with both processes resulting in similar seafloor morphologies. Time-lapse bathymetric surveys demonstrating migration direction are therefore essential when seeking to understand the characteristics of flows creating these features (Hage et al. 2018; Normandeau et al, 2020).

5.3. Depositional environments

These beds occur within successions dominated by thin-bedded and fine-grained turbidites and mass-transport deposits and are interpreted to represent proximal overbank deposits confined by an unstable lateral basin margin (Fig. 2) (Martínez-Doñate et al. 2023). Elsewhere in the depocentre, dune-prone units similar to those described here have been identified beneath coarse-grained channel-fills (Tek et al. 2020), lateral to channels (Bakke et al. 2008; Cornard and Pickering, 2019; Tek et al. 2020), and immediately upstream of fine-grained basinal mudstones (Mutti et al. 1977; Mutti and Normark, 1987), supporting the interpretation that these beds are the depositional remnants of flows that bypassed sediment at the mouths of channels and across the channel overbank areas (Mutti et al. 1977; Mutti and Normark, 1987) (Fig. 10; 11). Similar deep-marine dune or cross-stratified facies have been observed in the Cretaceous Lysing Formation, offshore Norway (Hansen et al. 2021), bottomsets of Miocene clinothems, offshore New Jersey (Stevenson et al. 2015; Hodgson et al. 2018), and in the Eocene-Oligocene Grès d'Annot of the Alpine foreland basin (Amy et al. 2000), and attributed to sediment bypass and reworking of the seabed by high-magnitude flows.

The presence of coarse-grained deposits lateral to channels indicates the parent flows were of a sufficiently high velocity to escape the channel thalweg confines without filtering out the coarse-grained fraction, suggesting that these deposits are representative of flows bypassing through the channel axis (Fig. 11) (e.g. McArthur et al. 2019). This is also supported by abundant *Thalassinoides* burrows on bed tops, which suggest high energy, axial environments (Heard and Pickering, 2008). These bedform-rich packages, therefore, provide an insight into the flows that cut the channels but that left little or no depositional trace within the channel thalweg itself (Englert et al. 2020). The poor preservation potential of these packages, coupled with the rare hydrodynamic conditions required for dune formation (e.g. Arnott, 2011; Tilston et al. 2015), may be the reason for the lack of dunes in ancient deep-water successions, as dune-bearing packages will be frequently cannibalised by avulsion or propagation of their associated channels (e.g. Hodgson et al. 2022), or simply not recognised at outcrop due to their relatively low thicknesses and affinity with weathered fine-grained sediments. The preservation potential of these deposits in the Aínsa Basin may have been favoured by enhanced lateral migration of channels adjacent to the thrust front (e.g. Bayliss and Pickering, 2015), resulting in channel mouths and overbanks being quickly abandoned and not cannibalised (Hodgson et al. 2022), high aggradation rates (Pemberton et al. 2016; Hodgson et al. 2022), early cementation aided by intense bioturbation and high bioclastic (and hence carbonate) content, or a combination of these factors.

362

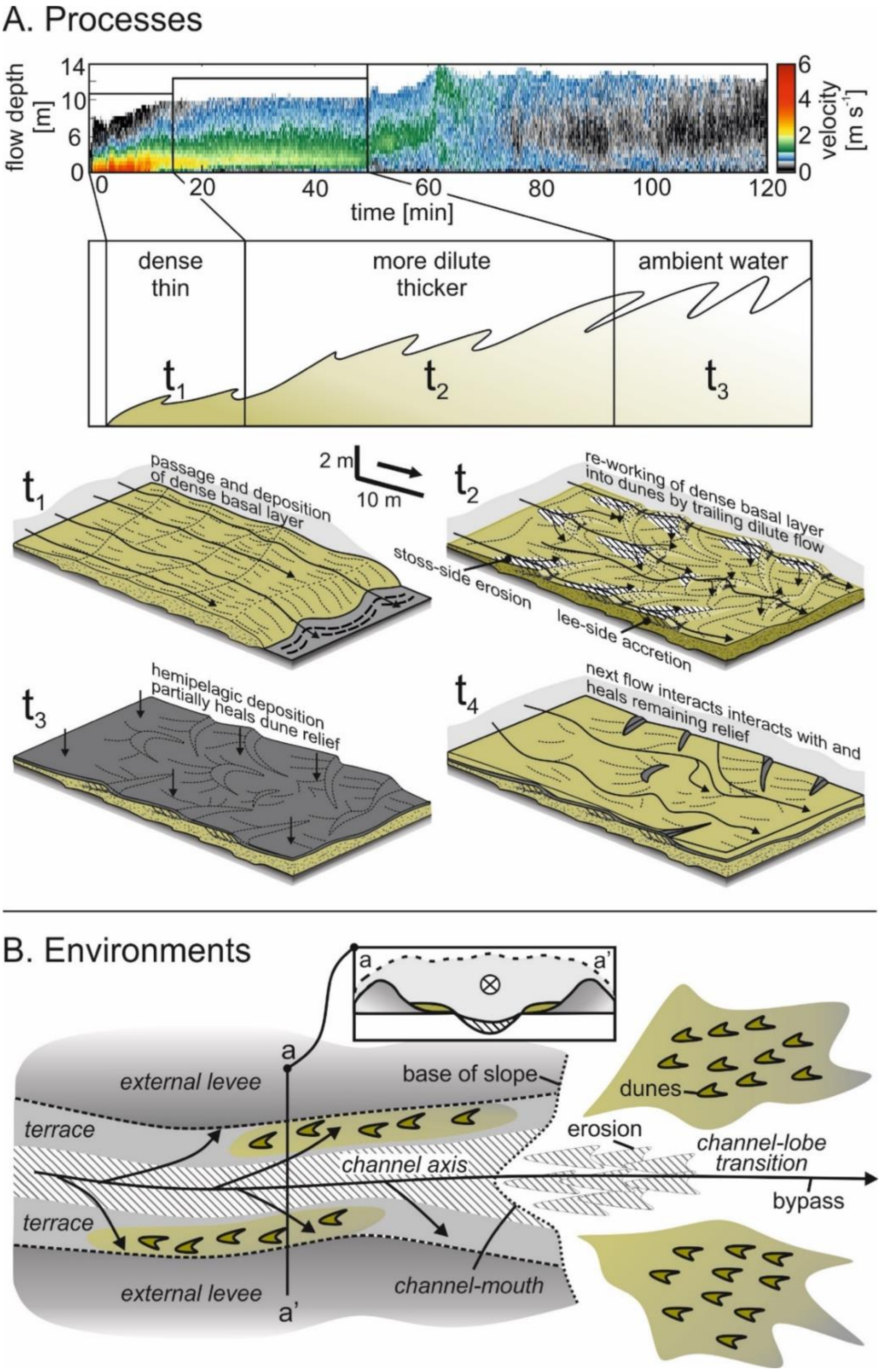

Figure 11. **A)** Sedimentary process model for the development of the deposits identified in this study, based on a synthesis of turbidity current direct measurements (modified from Pope et al. 2022). The dense basal layer is interpreted to have deposited the initial coarse-grained deposit before reworking the deposit into dunes by the body. The dunes are formed by lee-side accretion and stoss-side erosion, which form spoon-shaped scours. **B)** Depositional environments in which dunes are most likely to be developed in deep-marine environments.

6. Conclusion

Sedimentary bedforms are formed by fluids of particular properties and aid paleo-hydrodynamic reconstructions. One of the rarest bedforms found in exhumed deep-marine environments are dunes, resulting in the conditions required for their formation and preservation being uncertain when compared with other bedforms. Here, using Eocene deep-marine strata of the Aínsa Basin, Spain, we document the sedimentology of an extremely well-exposed package of three-dimensional coarse-grained dunes, which allows for the internal structure and paleoenvironmental significance of these bedforms to be investigated. The dune-bearing beds are composed of an inversely-graded, structureless division overlain by down-stream migrating dunes and scours, with superimposed fine-grained ripples formed on the dune stoss-sides. Following published direct measurements of turbidity currents, we interpret these dunes as having formed beneath the sustained body of high-magnitude turbidity currents, with the structureless division beneath the dunes representing the dense basal head of the current that was subsequently reworked. Scouring of dune stoss-sides during downstream migration and the development of superimposed ripples during flow waning modified the preserved dune shape, resulting in curvilinear dune crests and spoon-shaped scours being preserved in planform.

These dunes are associated with channelised environments and are interpreted to have been formed by flows that bypassed the channel axis and became depositional upon expanding across the channel overbank. Similar deposits have been identified elsewhere in the basin and interpreted to have been formed beneath high-magnitude flows that became similarly unconfined at the mouths of submarine channels or formed within scours. Where identified in the stratigraphic record, these dune-rich intervals may therefore represent the passage of high-magnitude turbidity currents and thus significant and geologically instantaneous bypass into the deep-basin.

7. Acknowledgements

Cai Puigdefàbregas and Dan Tek are thanked for discussions on the Aínsa Basin and its dunes. Dan Tek is thanked for sharing his and co-authors' figures on the Arro system. The authors thank the Slope project Phase 5 sponsors for financial support: BP, Aker BP, BHP, CNOOC, Hess, Murphy, Neptune Energy, Petrobras, Vår Energi, and Wintershall DEA.

8. Conflict of interest

The authors declare no conflict of interest.

9. Data availability

All dune measurements are available in the supplementary files.

10. Author contributions

ES: Conceptualization, data collection, data analysis, data interpretation, manuscript original draft

AMD: Conceptualization, data collection, data interpretation, manuscript review & editing

IK: Conceptualization, data collection, data interpretation, manuscript review & editing

MPM: Conceptualization, data interpretation, manuscript review & editing

WT: Data collection, data interpretation, manuscript review & editing

DH: Data collection, data interpretation, manuscript review & editing

MB: Data interpretation, manuscript review & editing

SF: Data interpretation, manuscript review & editing

References

Allen, J. R. L. (1982). Sedimentary structures, their character and physical basis, vol. 1. *Elsevier*, 593 p.

Amy, L.A., Kneller, B. and McCaffrey, W. (2000). Evaluating the links between turbidite characteristics and gross system architecture: upscaling insights from the turbidite sheet-system of Peïra Cava, SE France. *Deep Water Reservoirs of the World*, 1-15.

Arnott, R.W.C. (2012). Turbidites, and the case of the missing dunes. *Journal of Sedimentary Research*, *82*, 379-384

Arnott, R.W.C. and Al-Mufti, O. (2017). Deep-Marine Pseudo Dune Cross-Stratification—Similar, But Completely Different. *Journal of Sedimentary Research*, *87*, 312-323.

Baas, J.H., and Best, JL. (2002). Turbulence modulation in clay-rich sediment- laden flows and some implications for sediment deposition. *Journal of Sedimentary Research*, *72*, 336–340.

Baker, M.L. and Baas, J.H. (2020). Mixed sand–mud bedforms produced by transient turbulent flows in the fringe of submarine fans: Indicators of flow transformation. *Sedimentology*, *67*, 2645-2671.

Bakke, K., Gjelberg, J. and Petersen, S.A. (2008). Compound seismic modelling of the Aínsa II turbidite system, Spain: Application to deep-water channel systems offshore Angola. *Marine and Petroleum Geology*, *25*, 1058-1073.

Barnolas, A. and Teixell, A. (1994). Platform sedimentation and collapse in a carbonate-dominated margin of a foreland basin (Jaca basin, Eocene, southern Pyrenees). *Geology*, *22*, 1107-1110.

Bayliss, N. and Pickering, K.T., (2015). Transition from deep-marine lower-slope erosional channels to proximal basin-floor stacked channel–levée–overbank deposits, and syn-sedimentary growth structures, Middle Eocene Banastón System, Aínsa Basin, Spanish Pyrenees. *Earth-Science Reviews*, *144*, 23-46.

Bell, D., Stevenson, C.J., Kane, I.A., Hodgson, D.M. and Poyatos-Moré, M. (2018). Topographic controls on the development of contemporaneous but contrasting basin-floor depositional architectures. *Journal of Sedimentary Research*, *88(10)*, 1166-1189.

Blair, T.C. and McPherson, J.G. (1999). Grain-size and textural classification of coarse sedimentary particles. *Journal of Sedimentary Research*, *69*, 6-19.

Bouma, A.H. (1962). Sedimentology of Some Flysch Deposits: A Graphic Approach to Facies Interpretation. *Elsevier, Amsterdam*, 168 p.

Boulesteix, K., Poyatos-Moré, M., Flint, S.S., Taylor, K.G., Hodgson, D.M. and Hasiotis, S.T. (2019). Transport and deposition of mud in deep-water environments: Processes and stratigraphic implications. *Sedimentology*, *66*, p. 2894-2925.

[a]Cantalejo, B., Pickering, K.T., Miller, K.G. and Mac Niocaill, C. (2021). Chasing the 400 kyr pacing of deep-marine sandy submarine fans: Middle Eocene Aínsa Basin, Spanish Pyrenees. *Journal of the Geological Society*, *178*.

[b]Cantalejo, B., Pickering, K.T., McNiocaill, C., Bown, P., Johansen, K. and Grant, M. (2021). A revised age-model for the Eocene deep-marine siliciclastic systems, Aínsa Basin, Spanish Pyrenees. *Journal of the Geological Society*, *178*.

Cartigny, M.J. and Postma, G. (2017). Turbidity current bedforms, in Atlas of bedforms in the Western Mediterranean: *Springer, Cham*. 29 – 33.

Castelltort, S., Honegger, L., Adatte, T., Clark, J.D., Puigdefàbregas, C., Spangenberg, J.E., Dykstra, M.L. and Fildani, A. (2017). Detecting eustatic and tectonic signals with carbon isotopes in deep-marine strata, Eocene Aínsa Basin, Spanish Pyrenees. *Geology*, *45*(8), 707-710.

Chen, Y., Parsons, D.R., Simmons, S.M., Williams, R., Cartigny, M.J., Hughes Clarke, J.E., Stacey, C.D., Hage, S., Talling, P.J., Azpiroz-Zabala, M. and Clare, M.A. (2021). Knickpoints and crescentic bedform interactions in submarine channels. *Sedimentology*, *68*, 1358-1377.

Cisneros, J., Best, J., van Dijk, T., de Almeida, R.P., Amsler, M., Boldt, J., Freitas, B., Galeazzi, C., Huizinga, R., Ianniruberto, M. and Ma, H. (2020). Dunes in the world's big rivers are characterised by low-angle lee-side slopes and a complex shape. *Nature Geoscience*, *13*, 156-162.

Clarke, J.E.H. (2016). First wide-angle view of channelised turbidity currents links migrating cyclic steps to flow characteristics. *Nature Communications*, *7*, 1-13.

Collinson, J., and Mountney, N. (2019). Sedimentary Strctures 4th Edition. *Dunedin Academic Press*, 352 p.

Conway, K.W., Barrie, J.V., Picard, K. and Bornhold, B.D. (2012). Submarine channel evolution: active channels in fjords, British Columbia, Canada. *Geo-Marine Letters*, *32*, 301-312.

Cornard, PH and Pickering, K.T. (2019). Supercritical-flow deposits and their distribution in a submarine channel system, middle Eocene, Aínsa Basin, Spanish Pyrenees. *Journal of Sedimentary Research*, *89*, 576-597.

De Cala, I., Ohata, K., Dorrell, R., Naruse, H., Patacci, M., Amy, L.A., Simmons, S., McLelland, S.J. and McCaffrey, W.D. (2020). Relating the flow processes and bedforms of steady-state and waning density currents. *Frontiers in Earth Science*, *8*, 535743.

Dumas, S., Arnott, R.W.C. and Southard, J.B. (2005). Experiments on oscillatory-flow and combined-flow bed forms: implications for interpreting parts of the shallow-marine sedimentary record. *Journal of Sedimentary Research*, *75*, 501-513.

Englert, R.G., Hubbard, S.M., Matthews, W.A., Coutts, D.S. and Covault, J.A. (2020). The evolution of submarine slope-channel systems: Timing of incision, bypass, and aggradation in

Late Cretaceous Nanaimo Group channel-system strata, British Columbia, Canada. *Geosphere*, *16*, 281-296.

Fedele, J.J., Hoyal, D.C., Barnaal, Z., Tulenko, J., Awalt, S. (2016). Bedforms created by gravity flows. in Budd, D., Hajek, E., Purkis, S. (eds.), Autogenic Dynamics and Self-Organization in Sedimentary Systems. *SEPM Special Publication*, *106*, 95 -121.

Fernández, O., Muñoz, J.A., Arbués, P. and Falivene, O. (2012). 3D structure and evolution of an oblique system of relaying folds: the Aínsa basin (Spanish Pyrenees). *Journal of the Geological Society*, *169*, 545-559.

Ge, Z., Nemec, W., Vellinga, AJ and Gawthorpe, R.L. (2022).. How is a turbidite actually deposited? *Science Advances*, *8*, eabl9124.

Hansen, L.A.S., Hodgson, D.M., Pontén, A., Thrana, C. and Latre, A.O. (2021). Mixed axial and transverse deep-water systems: The Cretaceous post-rift Lysing Formation, offshore Norway. *Basin Research*, *33*, 2229-2251.

Hodgson, D.M., Browning, J.V., Miller, K.G., Hesselbo, S.P., Poyatos-Moré, M., Mountain, GS and Proust, J.N. (2018). Sedimentology, stratigraphic context, and implications of Miocene intrashelf bottomset deposits, offshore New Jersey. *Geosphere*, *14*, 95-114.

Hofstra, M., Hodgson, D.M., Peakall, J. and Flint, S.S. (2015). Giant scour-fills in ancient channel-lobe transition zones: Formative processes and depositional architecture. *Sedimentary Geology*, *329*, 98-114.

Hage, S., Cartigny, M.J., Clare, M.A., Sumner, E.J., Vendettuoli, D., Clarke, J.E.H., Hubbard, S.M., Talling, P.J., Lintern, D.G., Stacey, C.D. and Englert, R.G. (2018). How to recognise crescentic bedforms formed by supercritical turbidity currents in the geologic record: Insights from active submarine channels. *Geology*, *46*, 563-566.

Hand, BM. (1997). Inverse grading resulting from coarse-sediment transport lag. *Journal of Sedimentary Research*, *67*, 124-129.

Heard, T.G. and Pickering, K.T. (2008). Trace fossils as diagnostic indicators of deep-marine environments, Middle Eocene Aínsa-Jaca basin, Spanish Pyrenees. *Sedimentology*, *55(4)*, 809-844.

Heijnen, M.S., Clare, M.A., Cartigny, M.J., Talling, P.J., Hage, S., Lintern, D.G., Stacey, C., Parsons, D.R., Simmons, S.M., Chen, Y. and Sumner, E.J. (2020). Rapidly-migrating and internally-generated knickpoints can control submarine channel evolution. *Nature communications*, *11*, 1-15.

Hodgson, D.M., Peakall, J. and Maier, K.L. (2022). Submarine channel mouth settings: processes, geomorphology, and deposits. *Frontiers in Earth Science*. **10**, 790320.

Jobe, Z.R., Lowe, D.R. and Morris, W.R. (2012). Climbing-ripple successions in turbidite systems: depositional environments, sedimentation rates and accumulation times. *Sedimentology*, *59*, 867-898.

Kenyon, N.H., Akhmetzhanov, A.M. and Twichell, D.C. (2002). Sand wave fields beneath the Loop Current, Gulf of Mexico: reworking of fan sands. *Marine Geology*, *192*, 297-307.

Kneller, B.C. and McCaffrey, W.D. (2003). The interpretation of vertical sequences in turbidite beds: the influence of longitudinal flow structure. *Journal of Sedimentary Research*, *73*, 706-713.

Komar, P.D. (1985). The hydraulic interpretation of turbidites from their grain sizes and sedimentary structures. *Sedimentology*, *32*, 395-407.

Kuenen, P.H. and Migliorini, C.I. (1950). Turbidity currents as a cause of graded bedding. *The Journal of Geology*, *58*, 91-127.

Labaume, P., Mutti, E. and Seguret, M. (1987). Megaturbidites: a depositional model from the Eocene of the SW-Pyrenean foreland basin, Spain. *Geo-Marine Letters*, *7*, p. 91-101.

Läuchli, C., Garcés, M., Beamud, E., Valero, L., Honegger, L., Adatte, T., Spangenberg, J.E., Clark, J., Puigdefabregas, C., Fildani, A., de Kaenel, E., Hunger, T., Nowak, A., & Castelltort, S. (2021). Magnetostratigraphy and stable isotope stratigraphy of the middle-Eocene succession of the Ainsa basin (Spain): New age constraints and implications for sediment delivery to the deep waters. *Marine and Petroleum Geology*, *132*, 105182.

Le Roux, J.P. (2003). Can Dispersive Pressure Cause Inverse Grading in Grain Flows? Discussion. *Journal of Sedimentary Research*, *73*, 333-334.

Leeder, M.R. (1983). On the interactions between turbulent flow, sediment transport and bedform mechanics in channelised flows. *Modern and ancient fluvial systems,* 3-18.

Lowe, D.R. (1988). Suspended-load fallout rate as an independent variable in the analysis of current structures. *Sedimentology, 35*, 765-776.

Lucchi, F.R. and Valmori, E. (1980). Basin-wide turbidites in a Miocene, over-supplied deep-sea plain: a geometrical analysis. *Sedimentology*, *27*, 241-270.

Maier, K.L., Gales, J.A., Paull, C.K., Rosenberger, K., Talling, P.J., Simmons, S.M., Gwiazda, R., McGann, M., Cartigny, M.J., Lundsten, E. and Anderson, K. (2019). Linking direct measurements of turbidity currents to submarine canyon-floor deposits. *Frontiers in Earth Science*, *7*, 144.

Martínez-Doñate, A., Soutter E.L., Kane, I.A., Poyatos-More, M., Hodgson, D.M., Ayckbourne, A.J.M., Taylor, W.J., Bouwmeester, M.J., and Flint, S.S. (2022). Submarine crevasse lobes controlled by lateral slope failure in tectonically-active settings: an exhumed example from the Eocene Aínsa Basin, (Spain). *EarthArXiv*.

Meiburg, E. and Kneller, B. (2010). Turbidity currents and their deposits. *Annual Review of Fluid Mechanics*, *42*, 135-156.

Mochales, T., Barnolas, A., Pueyo, E.L., Serra-Kiel, J., Casas, A.M., Samsó, J.M., Ramajo, J. and Sanjuán, J. (2012). Chronostratigraphy of the Boltaña anticline and the Aínsa Basin (southern Pyrenees). *GSA Bulletin*, *124(7-8)*, 1229-1250.

Miramontes, E., Jorry, S.J., Jouet, G., Counts, J.W., Courgeon, S., Le Roy, P., Guerin, C. and Hernández-Molina, F.J. (2019). Deep-water dunes on drowned isolated carbonate terraces (Mozambique Channel, south-west Indian Ocean). *Sedimentology, 66,* 1222-1242.

Mutti, E. and Normark, W.R. (1987). Comparing examples of modern and ancient turbidite systems: problems and concepts, in Marine Clastic Sedimentology. *Springer, Dordrecht*, 1-38.

Mutti, E. (1992). Turbidite sandstones. *Agip S.p.A, Italy,* 275 p.

Mutti, E. (1977). Distinctive thin-bedded turbidite facies and related depositional environments in the Eocene Hecho Group (South-central Pyrenees, Spain). *Sedimentology, 24(1),* 107-131.

Mulder, T., Migeon, S., Savoye, B. and Faugères, J.C. (2001). Inversely graded turbidite sequences in the deep Mediterranean: a record of deposits from flood-generated turbidity currents? *Geo-marine letters, 21*, 86-93.

Normandeau, A., Bourgault, D., Neumeier, U., Lajeunesse, P., St-Onge, G., Gostiaux, L. and Chavanne, C. (2020). Storm-induced turbidity currents on a sediment-starved shelf: insight from direct monitoring and repeat seabed mapping of upslope migrating bedforms. *Sedimentology*, 67(2), 1045-1068.

Paull, C.K., Talling, P.J., Maier, K.L., Parsons, D., Xu, J., Caress, D.W., Gwiazda, R., Lundsten, E.M., Anderson, K., Barry, J.P. and Chaffey, M. (2018). Powerful turbidity currents driven by dense basal layers. *Nature communications, 9(1),* 1-9.

Pemberton, E.A., Hubbard, S.M., Fildani, A., Romans, B. and Stright, L. (2016). The stratigraphic expression of decreasing confinement along a deep-water sediment routing system: Outcrop example from southern Chile. *Geosphere*, *12*, 114-134.

Pickering, K.T. and Hiscott, R.N. (1985). Contained (reflected) turbidity currents from the Middle Ordovician Cloridorme Formation, Quebec, Canada: an alternative to the antidune hypothesis. *Sedimentology*, *32*, 373-394.

Pickering, K.T. and Bayliss, N.J. (2009). Deconvolving tectono-climatic signals in deep-marine siliciclastics, Eocene Aínsa basin, Spanish Pyrenees: Seesaw tectonics versus eustasy. *Geology*, *37*, 203-206.

Pope, E.L., Cartigny, M.J., Clare, M.A., Talling, P.J., Lintern, D.G., Vellinga, A., Hage, S., Açikalin, S., Bailey, L., Chapplow, N. and Chen, Y. (2022). First source-to-sink monitoring shows dense head controls sediment flux and runout in turbidity currents. *Science Advances*, *8*, eabj3220.

Puigdefàbregas, C., and Souquet, P. (1986). Tectono-sedimentary cycles and depositional sequences of the Mesozoic and Tertiary from the Pyrenees. *Tectonophysics*, 129, 173–203.

Reading, H.G. (2009). Sedimentary environments: processes, facies and stratigraphy. *John Wiley & Sons*. 688 p.

Remacha, E. and Fernández, L.P. (2003). High-resolution correlation patterns in the turbidite systems of the Hecho Group (South-Central Pyrenees, Spain). *Marine and Petroleum Geology*, *20*, 711-726.

Rodrigues, S., Hernández-Molina, F.J., Fonnesu, M., Miramontes, E., Rebesco, M. and Campbell, D.C. (2022). A new classification system for mixed (turbidite-contourite) depositional systems: Examples, conceptual models and diagnostic criteria for modern and ancient records. *Earth-Science Reviews*, 104030.

Schindler, R.J., Parsons, D.R., Ye, L., Hope, J.A., Baas, J.H., Peakall, J., Manning, A.J., Aspden, R.J., Malarkey, J., Simmons, S. and Paterson, D.M. (2015). Sticky stuff: Redefining bedform prediction in modern and ancient environments. *Geology*, *43*, 399-402.

Sequeiros, O.E., Spinewine, B., Beaubouef, R.T., Sun, T., Garcia, M.H. and Parker, G. (2010). Bedload transport and bed resistance associated with density and turbidity currents. *Sedimentology*, *57*, 1463-1490.

Simons, D.B., Richardson, E.V., and Haushild, W.L. (1963). Studies of Flow in Alluvial Channels, Some Effects of Fine Sediment on Flow Phenomena. *US Geological Survey Professional Paper*, *1489*, 46 p.

Southard, J.B. and Boguchwal, L.A. (1990). Bed configuration in steady unidirectional water flows; Part 2, Synthesis of flume data. *Journal of Sedimentary Research*, *60*, 658-679.

Stevenson, C.J., Talling, P.J., Masson, D.G., Sumner, E.J., Frenz, M. and Wynn, R.B. (2014). The spatial and temporal distribution of grain-size breaks in turbidites. *Sedimentology, 61*, 1120-1156.

Stevenson, C.J., Jackson, C.A.L., Hodgson, D.M., Hubbard, S.M. and Eggenhuisen, J.T. (2015). Deep-Water Sediment Bypass. *Journal of Sedimentary Research*, *85*, 1058-1081.

Sumner, E.J., Talling, P.J., Amy, L.A., Wynn, R.B., Stevenson, C.J. and Frenz, M. (2012). Facies architecture of individual basin-plain turbidites: Comparison with existing models and implications for flow processes. *Sedimentology*, *59*, 1850-1887.

Sylvester, Z. and Lowe, D.R. (2004). Textural trends in turbidites and slurry beds from the Oligocene flysch of the East Carpathians, Romania. *Sedimentology*, *51*, 945-972.

Talling, P.J., Baker, ML, Pope, EL, Ruffell, S.C., Jacinto, R.S., Heijnen, M.S., Hage, S., Simmons, S.M., Hasenhündl, M., Heerema, C.J. and McGhee, C. (2022). Longest sediment flows yet measured show how major rivers connect efficiently to deep sea. *Nature communications*, *13*, 1-15.

Tek, D.E., Poyatos-Moré, M., Patacci, M., McArthur, A.D., Colombera, L., Cullen, T.M. and McCaffrey, W.D. (2020). Syndepositional tectonics and mass-transport deposits control channelised, bathymetrically complex deep-water systems (Aínsa depocenter, Spain). *Journal of Sedimentary Research, 90*, 729-762.

Tilston, M., Arnott, R.W., Rennie, C.D. and Long, B. (2015). The influence of grain size on the velocity and sediment concentration profiles and depositional record of turbidity currents. *Geology*, v. *43(9)*, 839-842.

Todd, B.J. (2005). Morphology and composition of submarine barchan dunes on the Scotian Shelf, Canadian Atlantic margin. *Geomorphology*, *67*, 487-500.

Tsoar, H. (2001). Types of aeolian sand dunes and their formation. In: Geomorphological fluid mechanics. *Springer, Berlin, Heidelberg*, 403-429

Walker, R.G. (1965). The origin and significance of the internal sedimentary structures of turbidites. *Proceedings of the Yorkshire Geological Society, 35*, 1-32.

Walton, E.K. (1967). The sequence of internal structures in turbidites. *Scottish Journal of Geology*, *3*, 306-317.

Wynn, R.B., Masson, D.G. and Bett, B.J. (2002). Hydrodynamic significance of variable ripple morphology across deep-water barchan dunes in the Faroe–Shetland Channel. *Marine Geology*, *192(1-3)*, 309-319.

van Lunsen, H.A. (1970). Geology of the Ara-Cinca region, Spanish Pyrenees, province of Huesca. *Ph.D. thesis, Utrecht State University*, 119 p.